Rev. Roum. Sci. Techn.– Électrotechn. et Énerg.
Vol. **67**, *4*, pp. 389–394, Bucarest, 2022

EXPERIMENTAL ANALYSIS OF MULTILEVEL INVERTER-FED SIX-PHASE INDUCTION MOTOR FOR HIGH-POWER APPLICATIONS

VISHAL RATHORE[1], KRISHNA B. YADAV[2]

Keywords: Multilevel inverter; Pulse width modulation; Harmonic distortion; Six-phase induction motor.

This paper presents an implementation of a five-level cascaded H-bridge multilevel inverter (CHBMLI) fed six-phase induction motor (SPIM) for high-performance drive applications. The three-phase induction motor is modified to operate as SPIM to increase the reliability and enhance the performance of the motor. To maintain the speed of SPIM at a predefined value, fine-tuning of proportional-integral-derivative (PID) controlling parameters accomplished with closed-loop volts/Hertz control is proposed. Added to that, a phase disposition (PD) Pulse width modulation (PWM) technique and a low pass filter (LPF) are designed to get rid of the undesirable harmonics present in the output waveform of current and voltage. Matlab/Simulink platform is used to model the proposed topology. Simulation and experimental results show that the proposed PWM technique-based CHBMLI mitigates the current and voltage harmonics to 1.7 % and 7.20 %, respectively, and enhances the overall performance of the SPIM, which can be further employed for high-power industrial applications.

1. INTRODUCTION

Generally, most high-power variable speed motor drives use a multi-phase machine instead of the three-phase one due to its high torque density, high reliability, enhanced modularity, and greater efficiency [1,2]. The motivating progress in multi-phase machines is initiated by their prospective implementation in maritime, hybrid electric vehicles, aircraft, traction drives, and other high-power industrial applications. In general, high-power electrical drives require converters with high-frequency semiconductor switches, either unavailable in the market or expensive. This drawback is overcome by employing a multi-phase converter and multi-phase drives, which divides the power among the semiconductor devices. Thus, it reduces the current in each phase without a change in per-phase voltage [3]. This leads to the development of PWM-based MLI fed drives were reported in the literature [4]. The major benefit of using MLI over its two-level counterparts is its stepped output voltage, which lowers the requirement of the bulky transformer and thereby reduces the cost of the system employed for high-power applications [5]. MLI, combined with the multi-phase machine, results in a new arrangement of power segmentation that has increased power levels and a higher degree of freedom due to its flexible structure.

Also, the newly developed model allows the adaptation of control techniques and different modulation techniques to mitigate the harmonics and torque ripple with soft switching of the inverter switches [6]. The multi-phase machine can be set up with any number of phases from the traditional three-phase machine by spatially shifting stator winding by θ electrical degree. But the best performance is obtained in the case of the six-phase [7]. Therefore, SPIM is most frequently used for high-power applications. However, a SPIM fed by VSI introduces harmonics into the system, resulting in increased losses in the stator winding. Thus, a multilevel inverter (MLI) with suitable pulse width modulation (PWM) technique has been recognized as the viable solution to overcome the voltage and current harmonics of the switching converters in high-frequency, high-power applications [8].

This paper presents the mathematical modeling and performance analysis of CHBMLI fed six-phase drive. The PID controller is tuned to obtain the speed of the motor to a predefined value corresponding to the drive operating conditions. A closed-loop scalar volts/Hertz control is used to drive the SPIM, and an LPF is designed to eliminate the undesired harmonic content. Simulation results are well supported by experimental tests performed on a laboratory prototype which proves the correctness of the proposed scheme.

2. CASCADED H-BRIDGE MULTILEVEL INVERTER

The CHBMLI is more commonly used for industrial drive applications in multilevel inverters due to its ability to supply high power output. It eliminates the need for a coupling transformer to interface with a common connection point to the distribution network [9,10]. CHBMLI topology consists of serially connecting several H-bridge cells as shown in Fig. 1. A separate dc source V_{dc} is required to supply each cell to generate square wave output voltage $V_0(t)$, which is the cumulative output voltage of the H-bridge cell [11].

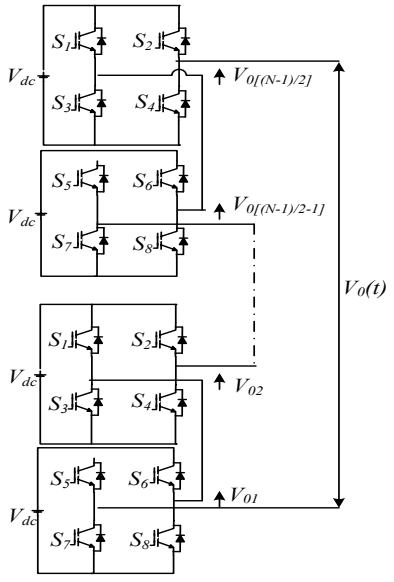

Fig. 1 – Cascaded H-Bridge Multilevel Inverter.

$$V_0(t) = V_{01}(t) + V_{02}(t) + \ldots \ \ldots \ \ldots + V_{0N}(t). \qquad (1)$$

[1] Department of Electrical Engineering, NIT Jamshedpur, Jharkhand India-831014, E-mail: vishalrathore01@gmail.com, kbyadav.ee@nitjsr.ac.in

$$V_0(t) = \sum_{i=1}^{N} (P_i - 1)\ V_{dc,i}\ , \tag{2}$$

where, $P_i = 0,1,2,...$

3. SIX-PHASE INDUCTION MOTOR MODEL

The stator and rotor windings of a SPIM in a *q-d* reference frame are shown in Fig. 2. V_{r1}, V_{r2}, V_{r3}, V_{r4}, V_{r5}, V_{r6}, and V_{s1}, V_{s2}, V_{s3}, V_{s4}, V_{s5}, V_{s6} are the six-phase voltages of rotor and stator winding, respectively. θ is the rotational angle between the stator winding and the reference frame. The *q-d* axis frame rotates at an angular speed ω_r inside the rotor to avoid the time change inductance in the output voltage [12].

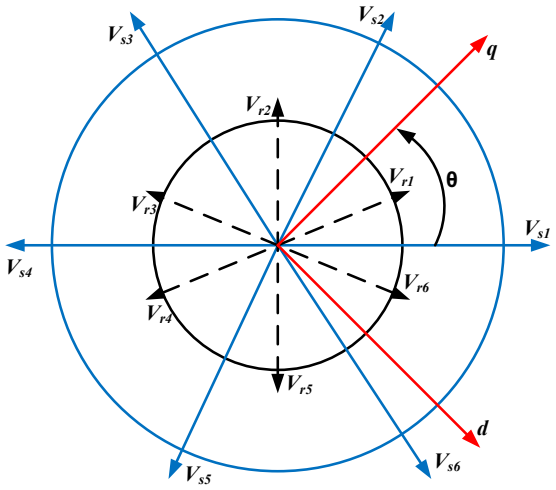

Fig. 2 – Representation of stator and rotor winding in the *q-d* frame.

The sinusoidal voltages of SPIM are represented as:

$$V_{s1} = V_m \sin(\omega t)\,. \tag{3}$$

$$V_{s2} = V_m \sin\left(\omega t - \frac{\pi}{3}\right). \tag{4}$$

$$V_{s3} = V_m \sin\left(\omega t - \frac{2\pi}{3}\right). \tag{5}$$

$$V_{s4} = V_m \sin(\omega t - \pi). \tag{6}$$

$$V_{s5} = V_m \sin\left(\omega t - \frac{4\pi}{3}\right). \tag{7}$$

$$V_{s6} = V_m \sin\left(\omega t - \frac{5\pi}{3}\right). \tag{8}$$

The transformation voltage V_q and V_d of the *q-d* axis is expressed as [7]:

$$V_q = \frac{1}{3}\left[\sum_{k=1}^{6} V_k Cos\left(\theta - \frac{(k-1)\pi}{6}\right)\right]. \tag{9}$$

$$V_d = \frac{1}{3}\left[\sum_{k=1}^{6} V_k Cos\left(\theta - \frac{(k-1)\pi}{6}\right)\right]. \tag{10}$$

The *q-d* axis stator flux (ψ_{qs}, ψ_{ds}) and current component (i_{qs}, i_{ds}) are given by:

$$\psi_{qs} = \frac{1}{s}\left[-\omega_e \psi_{ds} - R_s i_{qs} + V_{qs}\right]. \tag{11}$$

$$\psi_{ds} = \frac{1}{s}\left[-\omega_e \psi_{qs} - R_s i_{ds} + V_{ds}\right]. \tag{12}$$

$$i_{qs} = \frac{1}{L_s}\left[\psi_{qs} - L_m i_{qr}\right]. \tag{13}$$

$$i_{ds} = \frac{1}{L_s}\left[\psi_{ds} - L_m i_{dr}\right]. \tag{14}$$

The *q-d* axis rotor flux (ψ_{qr}, ψ_{dr}) and current component (i_{qr}, i_{dr}) are expressed as

$$\psi_{qr} = \frac{1}{s}\left[(\omega_r - \omega_e)\psi_{dr} - R_r i_{qr}\right]. \tag{15}$$

$$\psi_{dr} = \frac{1}{s}\left[(\omega_e - \omega_r)\psi_{qr} - R_r i_{dr}\right]. \tag{16}$$

$$i_{qr} = \frac{1}{L_r}\left[\psi_{qr} - L_m i_{qs}\right]. \tag{17}$$

$$i_{dr} = \frac{1}{L_r}\left[\psi_{qr} - L_m i_{ds}\right]. \tag{18}$$

The Electrical torque (T_e) and rotor electrical speed (ω_e) are formulated as:

$$T_e = \frac{3p}{2}\left[\psi_{ds} i_{qs} - \psi_{qs} i_{ds}\right]. \tag{19}$$

$$\omega_e = \frac{p}{2s}\left[\frac{1}{J}\left(T_e - T_L - D\frac{2}{p}\omega_e\right)\right]. \tag{20}$$

$$n_r = \frac{2}{p}\frac{60}{2\pi}\omega_e\ . \tag{21}$$

$$\text{If } \theta = 0, \text{ then } \omega_e = 0. \tag{22}$$

The electrical torque is reformulated as:

$$T_e = \frac{3p}{4}\left[\lambda_{ds} I_{qs} - \lambda_{qs} I_{ds}\right], \tag{23}$$

where p is the number of the pole, D is the damping factor, L_s and L_r are the stator and rotor inductance [H], L_m is the magnetizing inductance [H], ω_e is the rotor electrical speed, n_r is the angular speed in rpm, λ_{qs} and λ_{ds} are the stator flux linkage of the *q-d* frame, T_L is the load torque.

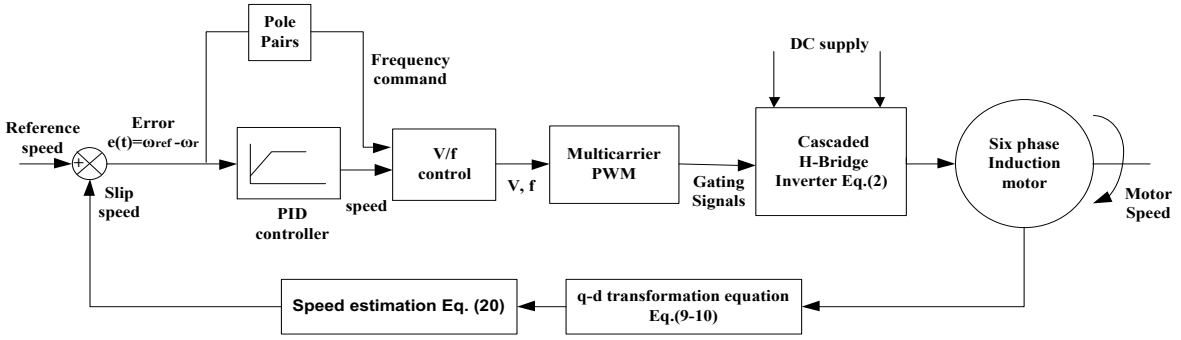

Fig. 3 – Block diagram of proposed PID controller-based closed-loop volts/hertz control.

4. DESIGN PROCEDURE OF PROPOSED PID CONTROLLER

The closed-loop volts/hertz control technique is simple and has good accuracy of motor speed. In this method, the decrease in motor speed causes an increase of flux, resulting in high magnetizing current, poor condition of pole saturation, and thereby falling power factor [13,14]. The proposed PID control strategy performs two tasks. The first is to estimate the speed, and the second is to robustly perform closed-loop control of SPIM. Figure 3 shows the proposed closed-loop PID-based control scheme of SPIM.

4.1 ESTIMATION OF SPEED

The proposed speed estimation scheme is less complex and more economical that utilizes the SPIM parameters and estimating flux linkage at any speed, as shown by the flow chart in Fig. 4.

The voltages of the *q*-axis and *d*-axis on the stator side of the motor terminals can be expressed as:

$$V_{qs} = R_s I_{qs} + p\lambda_{qs} - \omega\lambda_{ds} \ . \tag{24}$$

$$V_{ds} = R_s I_{ds} + p\lambda_{ds} - \omega\lambda_{qs} \ . \tag{25}$$

The component of flux derivative can be completed as:

$$\lambda'_{qr} = \left[\frac{L_r}{L_m} \left(V_{qs} - I_{qs} \right) R_s + \sigma L_s s \right] . \tag{26}$$

$$\lambda'_{dr} = \left[\frac{L_r}{L_m} \left(V_{ds} - I_{ds} \right) R_s + \sigma L_s s \right] . \tag{27}$$

The flux component can be:

$$\lambda_{qr} = p\lambda'_{qr} \ . \tag{28}$$

$$\lambda_{dr} = p\lambda'_{dr} \ . \tag{29}$$

The estimated speed is given by**:**

$$\omega_r = \frac{1}{\lambda_r^2} \left[\left(\lambda_{dr}\lambda'_{qr} - \lambda_{qr}\lambda'_{dr} \right) - \frac{L_m}{T_r} \left(\lambda_{dr} I_{qs} - \lambda_{qr} I_{ds} \right) \right] \tag{30}$$

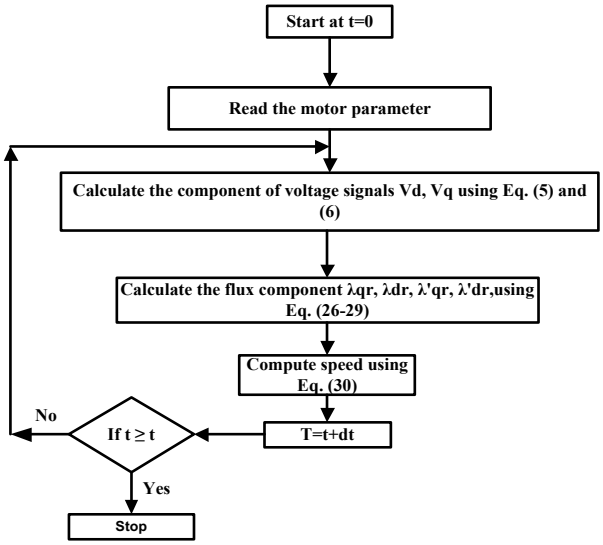

Fig. 4 – Flow chart for speed estimation.

$$\sigma = 1 - \frac{L_m^2}{LrLs} \ . \tag{31}$$

$$\lambda_r^2 = \lambda_{qr}^2 + \lambda_{dr}^2 \ . \tag{32}$$

$$T_r = \frac{L_r}{R_r} , \tag{33}$$

where σ is the leakage coefficient, s is the Laplace operator, λ_{qr} and λ_{dr} are the rotor flux linkage of the q-d frame, and *p* denote differentiation that is $p = \mathrm{d}/\mathrm{d}t$.

5. CLOSED LOOP CONTROL SYSTEM

To see the performance analysis of the machine, a closed-loop volts/hertz control is employed. The controller's estimated speed output is given as the input to the closed-loop system.

$$e(t) = \omega_{ref} - \omega_r \ . \tag{34}$$

The tuning of the PID controller is dependent on the speed error signal such that it compensates for the error in speed by generating the required frequency deviation in the stator of the SPIM. The feedback signal in closed-loop volts/hertz control is obtained from the motor parameters, which measure the voltages and currents. The PID controller tuning is based on the three parameters Kd, Ki, and Kp, which are calculated using Ziegler-Nichols and

approximation methods.

$$u(t) = k_p e(t) + k_d \frac{de(t)}{dt} - k_i \int e(t)dt\,, \tag{35}$$

where derivative gain $K_d = K_p$. T_d, and integral gain $K_i = K_p/T_i$ in which K_p is the proportional gain, T_d is the derivative time constant, and T_i is the integral time constant.

By Laplace transform, the PID controller is defined as:

$$G(s) = k_p\left(1 + k_d s + \frac{1}{T_i s}\right). \tag{36}$$

The two signals known as speed error and error in speed are the input of the PID controller resulting in tuned control parameters fed to the cascade H-Bridge inverter. The maxima and minima of K_p and K_d are practically determined, and for ease of simplification, they are normalized in the range from 0 to 1 and are given by the following sets of equations as

$$k'_p = \left(\frac{k_p - k_{p\min}}{k_{p\max} - k_{p\min}}\right). \tag{37}$$

$$k'_d = \left(\frac{k_d - k_{d\min}}{k_{d\max} - k_{d\min}}\right). \tag{38}$$

$$T_i = \alpha T_d\,. \tag{39}$$

$$k_i = \frac{k_p}{\alpha T_d} = \frac{k_p^{\,2}}{\alpha k_d}\,. \tag{40}$$

6. SIMULATION RESULTS

For analyzing the proposed scheme, MATLAB/Simulink environment is used to model CHBMLI-fed SPIM. The five-level output voltage of CHBMLI using PD topology is shown in Fig. 5.

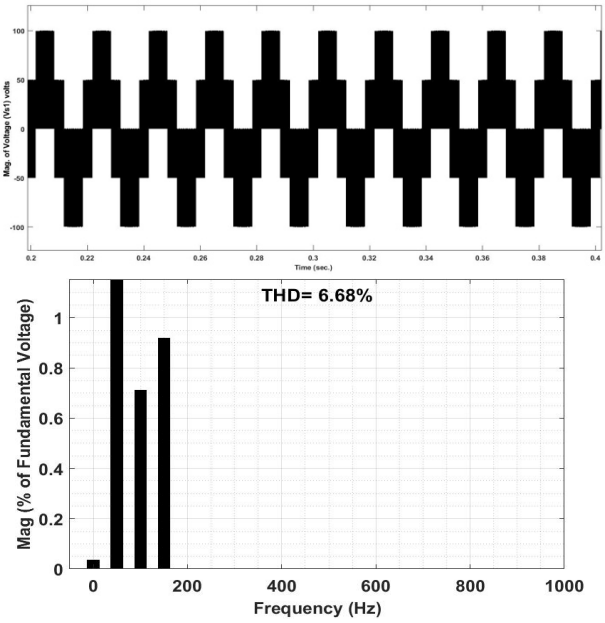

Fig. 5 – Five level output of CHBMLI and its harmonic content.

It has been observed that the line to neutral voltage of the inverter has harmonic content of 6.68 %. Figure 6 shows the variation of the current I_q and I_d in the *q-d* axis frame. The dynamics of the drives usually change with the input frequency, and the sequential response of closed-loop volts/hertz control is classified and studied in four cases shown in Table 1. The controller which controls the speed works with the proposed PID controller. The parameters of SPIM are tabulated in Table 2**.**

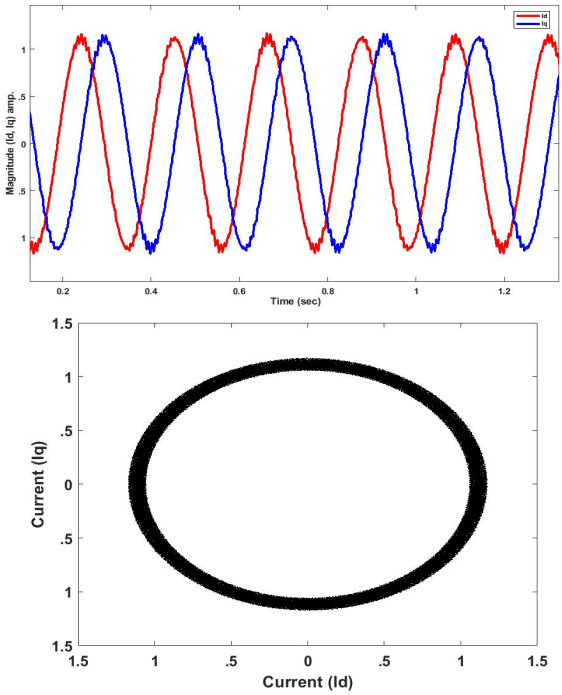

Fig. 6 – Variation of current I_q *and* I_d in the *q-d* reference frame.

Table 1

Operating Sequence of SPIM implemented with PID controller

Cases	Time Period		Remark
	From	To	
1	0.0	0.3	Starting time
2	0.3	0.5	Normal Operation
3	0.5	0.7	Reduce speed (load applied)
4	0.7	2	Back to normal operation

Table 2

Parameters of SPIM

Power (P)	1HP	Stator resistance (R_s)	4Ω
Voltage (V)	220 v	Rotor resistance (R_r)	4Ω
Frequency (f)	50 Hertz	Mutual Inductance (L_m)	782.7 mH
Speed (ω_r)	1500 rpm	Stator and Rotor Inductance (L_s, L_r)	808.17 mH
Current (i)	1.8 Amp	Moment of Inertia(J)	.0088 Kg-m2

Figure 7 shows the variation of speed using the PID controller. The controller clears the effectiveness of speed estimation of SPIM as the estimated speed is close to the actual speed. The motor has better performance in terms of settling time and rise time. Figure 8 shows the variation of torque for the above studied. The closeness between the developed mechanical torque (T_m) and electric torque (T_e) is apparent. At time = 0.6 s, a load torque of 4 Nm is applied, slightly reducing the motor speed. Figure 9 shows the variation of close loop stator current I_{s1} as a function of time during load and no-load conditions, having a THD of 1.52 %.

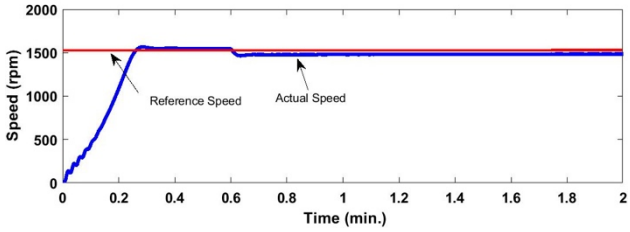

Fig. 7 – Speed characteristic of SPIM as a function of time.

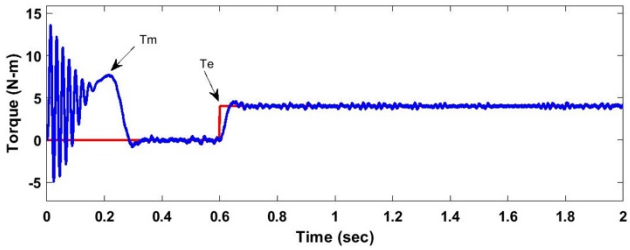

Fig. 8 – Variation of torque as a function of time.

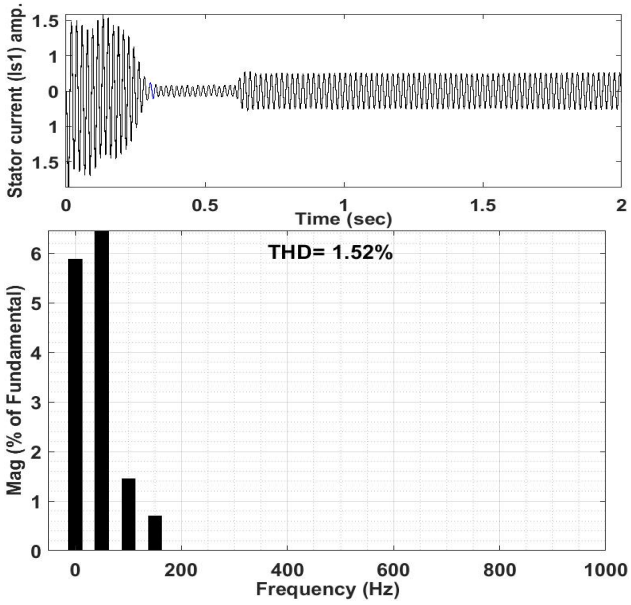

Fig. 9 – Steady-state stator current (I_{s1}) and its harmonic content.

7. EXPERIMENTAL RESULTS

The experimental setup of a laboratory prototype is shown in Fig. 16. A digital signal processor TMS320F28334 is used to initiate the modulation process, which works as a controller. IGBT SKM50GB123D model capable to withstand 1200 V, 50 A is used as a switch for a five-level inverter connected to a 1 HP, 4 Pole six-phase induction motor. A dc voltage of 600 V is supplied from a bulky autotransformer. A pulse from a real-time controller dSPACE DS1102 is used to drive the gate circuit. Current sensor LEM makes LA 25 NP, and voltage sensor LV 10-1000 are used to measure the value of current and voltages. Hardware results of the proposed scheme are presented in Fig. 10 to Fig. 15. All the results are recorded and analyzed by a digital storage oscilloscope Yokogawa DL750. Fig. 10 shows the five-level line to a neutral output voltage of the cascaded multilevel inverter. The output voltage has a Total Harmonic Distortion (THD) of 7.2 %. Also, from Fig. 11, the proposed scheme suppressed the odd number of harmonics.

Figure 12 shows the speed and current characteristics through CH1, CH2, and CH3, respectively. In Fig. 13, channel CH1 is the electromagnetic torque (T_e), and CH2 is the mechanical torque (T_m). The closeness of characteristics clears the effective implementation of the proposed work. Figure 14 shows the variation of the six-phase close-loop stator current and the zoomed view, scaled down to 1/2. Harmonic present in the stator current is recorded and shown in Fig. 15. Table 3 shows the assessment of PID-fed SPIM based on the trial-and-error method.

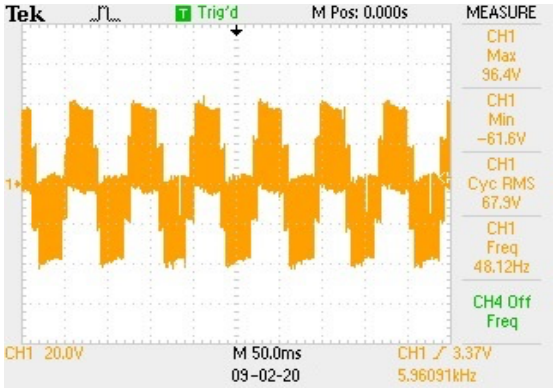

Fig. 10 – Five-level output voltage of CHBMLI.

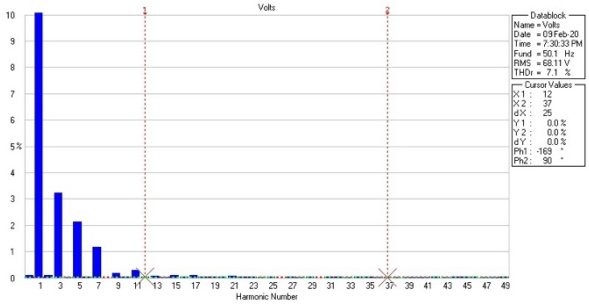

Fig. 11 – Harmonic profile of output voltage.

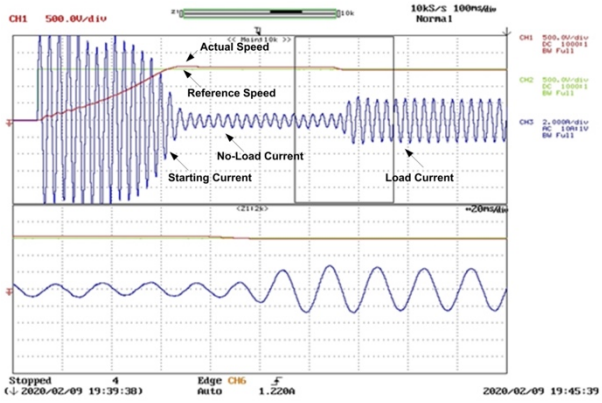

Fig. 12 – Current and speed characteristics of SPIM.

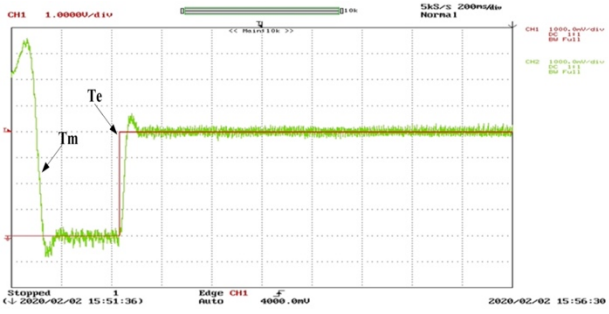

Fig. 13 – Torque profile of close loop control SPIM.

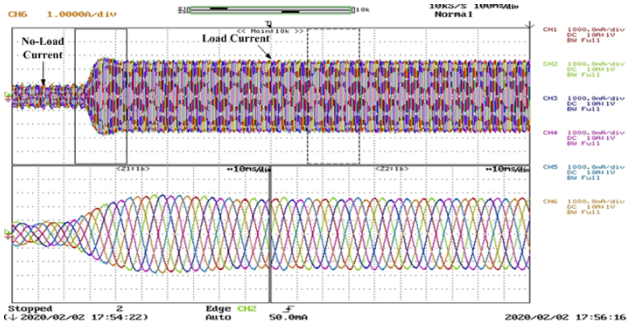

Fig. 14 – Steady-state six-phase stator current.

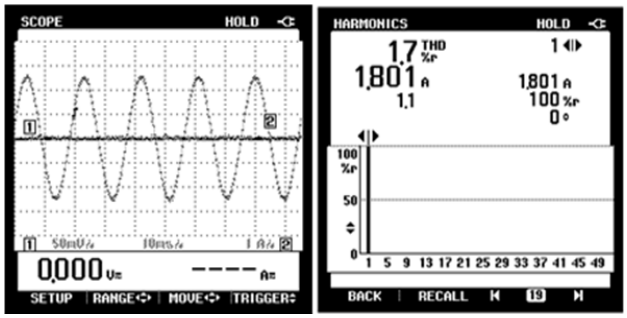

Fig. 15 – Stator current (I_{s1}) and THD content.

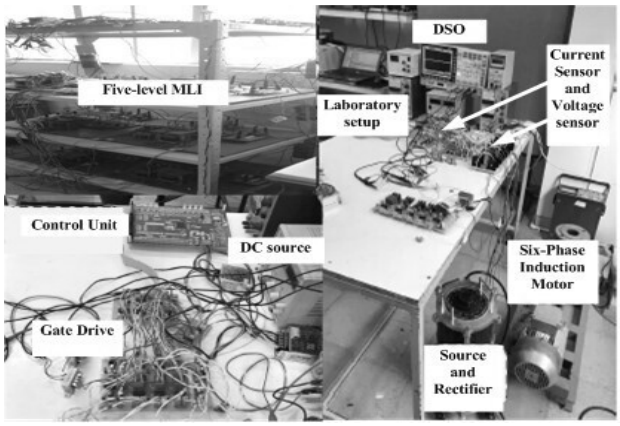

Fig. 16 – Experimental set-up.

Table 3

Operating Sequence of SPIM implemented with PID controller

Index		Current (A)	Speed (rpm)	Estimated speed (rpm)	THD (%)	Rise time
Case I	Overshoot	1.8	1499	1492	1.7	0.03
	Steady state error	0.2	1	8	0.1	-
Case II	Overshoot	1.6	1496	1487	1.5	0.06
	Steady state error	0.4	4	13	0.3	-

8. CONCLUSIONS

This paper presents an implementation and detailed analysis of CHBMLI-fed SPIM. A PD topology and its implementation based on MLI using PID-based scalar volts/hertz close-loop control have been proposed. The results show that CHBMLI with a suitable PWM technique reduces the torque ripple and lowers the current and voltage harmonics. It is clear from the analysis that the proposed PID controller-based scheme enhanced the system's performance. It has been observed that the tuned PID controller reduces the overshoot and steady-state error lowers the current harmonics to 1.5-1.7 %, which is under the permissible limit and provides uniform performance of the drive over the entire speed range. Moreover, the feedback loop reduces settling time to 4-5 % and provides better speed regulation. Hence, the feasibility of the proposed scheme is well supported by experimental analysis.

Received on 25 January 2021

REFERENCES

1. E. Levi, *Multiphase electric machines for variable-speed applications*, IEEE Trans. Ind. Electron., **55**, *5*, pp. 1893-1909 (2008).
2. K.A. Chinmaya, G.K. Singh, *Experimental analysis of various space vector pulse width modulation (SVPWM) techniques for dual three-phase induction motor drive,* International Transactions on Electrical Energy Systems, **29**, *1*, e2678 (2019).
3. E. Levi, R. Bojoi, F. Profumo, H.A. Toliyat, S. Williamson, *Multi-phase induction motor drives–a technology status review*, IET Electric Power Applications, **1**, *4*, pp. 489-516 (2007).
4. D. Casadei, G. Serra, A. Tani, L. Zarri, *General inverter modulation strategy for multi-phase motor drive,* IEEE International Symposium on Industrial Electronics, pp. 1131-1137, 2007 June 4.
5. J. Rodriguez, J.S. Lai, F.Z. Peng, *Multilevel inverters: a survey of topologies, controls, and applications*, IEEE Transactions on industrial electronics, **49**, *4*, pp. 724-38 (2002).
6. M. Malinowski, K. Gopakumar, J. Rodriguez, M.A. Perez, *A survey on cascaded multilevel inverters*, IEEE Transactions on industrial electronics, **57**, *7*, pp. 2197-2206 (2009).
7. V. Rathore, K.B. Yadav, *Comparative efficiency analysis of five-level dual three-phase multilevel inverter fed six-phase induction motor drive*, International Journal of Numerical Modelling: Electronic Networks, Devices, and Fields, e2981, (2021).
8. O. Dordevic, M. Jones, E. Levi, *A comparison of carrier-based and space vector PWM techniques for three-level five-phase voltage source inverters*, IEEE Transactions on Industrial Informatics, **9**, *2*, pp. 609-619 (2012).
9. J. Tandekar, A. Ojha, S. Jain, *Five-level cascaded H-bridge MLC-based shunt active power filter for active harmonics mitigation in distributed network*, Journal of Circuits, Systems, and Computers, **28**, *2*, pp. 1950035 (2019).
10. F. Chabni, R. Taleb, M. Helaimi, *Output voltage waveform improvement of modified cascaded H-bridge multilevel inverter using selective harmonic elimination technique based on hybrid genetic algorithm*. Rev. Roum. Sci. Techn. – Électrotechn. Et Énerg., **62**, *4*, pp. 405-410 (2017).
11. K. Iffouzar, M.F. Benkhoris, K. Ghedamsi, D. Aouzellag, *Behavior analysis of a dual stars induction motor supplied by PWM multilevel inverters*, Rev. Roum. Sci. Techn. – Électrotechn. Et Énerg., **61**, *2*, pp. 137-141 (2016).
12. V. Rathore, K.B. Yadav, *Analytical model-based performance characteristics analysis of six-phase induction motor*, Proceedings of the International Conference on Advances in Electronics, Electrical & Computational Intelligence (ICAEEC) (2020).
13. A. Datta, G. Poddar, *Improved low-frequency operation of hybrid inverter for medium voltage induction motor drive under V/f and vector control mode of operation*. IEEE Journal of Emerging and Selected Topics in Power Electronics, **8**, *2*, pp. 1248-1257 (2019).
14. A. Chitra, J. Vanishree, S. Sreejith, S. Jose, A.J. Pulickan, *Performance comparison of multilevel inverter topologies for closed loop V/f controlled induction motor drive*, Energy Procedia. **117**, pp. 958-965 (2017).